Raman spectra of Ag_xTiS_2 and lattice dynamics of TiS_2

S. Jiménez Sandoval,* X. K. Chen, and J. C. Irwin
Department of Physics, Simon Fraser University, British Columbia, Canada V5A 1S6
(Received 13 December 1991)

Raman-scattering experiments have been carried out on stage-2 silver-intercalated TiS_2 single crystals. Below a transition temperature near 300 K, the intercalated silver atoms become ordered in a structure that produces a $\sqrt{3}a\times\sqrt{3}a\times 2c$ superlattice. Besides the Raman-allowed E_g and A_{1g} modes of TiS_2, we have observed nine additional modes in the Raman spectra of the ordered phases of the intercalated crystals. These modes are zone folded from the K and A points of the original Brillouin zone. Using the frequency of these Raman modes and the available infrared and neutron-scattering data, the phonon-dispersion curves and phonon frequency distribution of TiS_2 have been calculated within the approximation of a valence-force-field lattice-dynamics model.

I. INTRODUCTION

Titanium disulfide (TiS_2) is an indirect-gap semiconductor and a member of the family of layered transition-metal dichalcogenides. Its structure consists of TiS_2 layers separated by a van der Waals–type interlayer gap. One interesting characteristic of this semiconductor is its peculiarity of presenting in-plane semimetallic properties such as the temperature dependence of the electrical resistivity, $\rho=\rho_0+aT^p$, where p varies approximately between 1.6 and 2.3 depending upon excess Ti content,[1] and of the thermoelectric power α, which is proportional to T. The semimetallic behavior of TiS_2 is due to the high density of free carriers which, depending upon sample stoichiometry, lies in the 10^{20}–10^{21} cm^{-3} range.[1] In a recent study, Molenda *et al.*[2] concluded that the high electrical conductivity of TiS_2 is due to the contribution of extrinsic carriers, provided by excess Ti ions which occupy sites within the interlayer gap,[3] and of thermally excited electrons independent of sample stoichiometry.[2]

Several experimental techniques have been employed to study the lattice dynamics of TiS_2. The infrared-active E_u mode has been reported by Vaterlaus and Levy[4] at 158 cm^{-1} and by Lucovsky *et al.*[5] at 175 cm^{-1}. Raman measurements[6] yielded the frequencies for the E_g and A_{1g} modes at 232 and 336 cm^{-1}, respectively. Schärli and Lévy[7] performed inelastic neutron-scattering experiments to study the dispersion of acoustic phonons in the $\Gamma-A$ direction of the Brillouin zone. They[7] did not find any evidence of the zone-boundary phonon previously predicted by Kaveh, Cherry, and Weger,[8] who proposed an electron-phonon scattering mechanism via a second-order coupling to an LA interlayer mode to explain the nearly quadratic temperature dependence of the electrical resistivity in TiS_2. They estimated that the phonon involved in this process should have an energy of about 2 meV at the zone boundary $(0,0,\pi/c)$. More recently, Negishi *et al.*[9] studied the effect of intercalation on the tunneling characteristics of TiS_2. Their measurements allowed them to estimate various phonon frequencies and deduce a set of dispersion curves for vibrational energies less than 25 meV.

TiS_2 can be intercalated with various metals[10–19] to create systems with a wide variety of physical properties. The dynamics of the atoms between the host layers is one of the most interesting features of these systems, and it has been the subject of several investigations.[13–16,20,21] The intercalation of silver atoms between the TiS_2 layers (Ag_xTiS_2) produces stage-1 and/or stage-2 intercalates[14] within specific ranges of temperature and silver concentration.[20] In Ag_xTiS_2 the silver atoms undergo an order-disorder phase transition below room temperature that has been studied experimentally by several techniques such as electron[6] and x-ray diffraction[22,23] and by Raman spectroscopy.[6,15,16] In the ordered phase the intercalated silver atoms occupy sites with octahedral symmetry[22] located midway between Ti atoms of the adjacent layers, resulting in the formation of a $\sqrt{3}a\times\sqrt{3}a\times 2c$ superlattice.

In the present work a detailed Raman study has been performed on stage-2 $Ag_{1/3}TiS_2$ and $Ag_{0.16}TiS_2$ single crystals. Additional Raman peaks associated with zone-boundary phonons are observed in the spectra as a consequence of the zone-folding mechanism that occurs when the $a\sqrt{3}\times a\sqrt{3}\times 2c$ superlattice is formed. By using the available neutron-scatttering data,[7] the frequency of the infrared mode[5] E_u and the zone-folded Raman frequencies measured in this work, the phonon dispersion curves and density of states of TiS_2 have been calculated within the approximation of a valence-force-field (VFF) lattice-dynamics model.

II. EXPERIMENTAL DETAILS

The Raman-scattering experiments were carried out on different samples that were prepared following the procedure described by Gerards *et al.*[22] Briefly, appropriate proportions of TiS_2 and Ag powders were heated in evacuated quartz ampoules at a temperature of 1000 K for periods of three to four days. The crystals obtained were powdered and reheated for three days at 1000 K and then allowed to cool to room temperature.

X-ray diffraction patterns of the samples were obtained using a Phillips vertical circle diffractometer and showed only (001) peaks, and in particular, the (003) line characteristic of stage-2 Ag_xTiS_2.[14] The c spacing determined from the x-ray measurements was 12.153 ± 0.005 Å for samples with $x=0.33$ and 12.135 ± 0.005 Å for samples with $x=0.16$. These values are consistent with those determined by Scholz and Frindt[14] in samples with similar silver concentrations.

The Raman spectra were obtained by exciting the samples with the 488.0- or 514.5-nm lines of an argon-ion laser beam focused on the sample surface with the aid of a cylindrical lens. The scattered light was then collected in a near-backscattering configuration and concentrated at the entrance slit of a computer-controlled triple spectrometer. The signals were analyzed with an ITT Mepsicron imaging detector, and the data were stored and processed in an IBM PC microcomputer. The spectra were obtained at various temperatures in the region from 15 to 296 K by mounting the samples on the cold finger of a Displex refrigerator with the a-b planes of the samples parallel to the sampler holder surface. We have labeled the laboratory coordinate axes as Y and X indicating vertical and horizontal axes, respectively.

In this paper we report the presence of several features in the low-temperature spectra that were not observed in previous experiments.[15,16] Two factors have led to the observation of additional features in the spectra obtained from the intercalated crystals at temperatures below 280 K. First, our present Raman system provides a sensitivity and signal-to-noise ratio that are significantly enhanced with respect to those used in earlier experiments.[6,15,16] Second, the single crystals used in the present work have much higher-quality surfaces than those of the electrochemically intercalated crystals utilized in previous Raman studies.

III. RESULTS

A. Raman scattering of stage-2 silver-intercalated TiS_2

Raman spectroscopy has been employed in the past to study the lattice dynamics and the order-disorder phase transition in silver-intercalated TiS_2. Besides the E_g and A_{1g} Raman active zone-center modes predicted by group theory for TiS_2, four extra peaks were reported in the previous Raman-scattering studies.[6,15,16] The additional modes had frequencies of 128 (A_1), 272 (A_2), and 306 cm^{-1} (A_3) in spectra obtained at 100 K (Ref. 15) and also 207 cm^{-1} in experiments[6] carried out at 4.2 K. The appearance of these peaks was explained in terms of a reciprocal-space zone-folding mechanism[15] that occurred as a consequence of the ordering of the silver atoms in a $a\sqrt{3}\times a\sqrt{3}\times 2c$ superlattice. Indeed, the original Brillouin zone and that of the $a\sqrt{3}\times a\sqrt{3}\times 2c$ superlattice are related in such a way that the new zone center coincides[15] with the points K and A of the hexagonal Brillouin zone of the unintercalated crystal. Therefore, zone-boundary phonons with wave vectors $\mathbf{q}=\frac{1}{3}(\mathbf{a}^*+\mathbf{b}^*)$ (K point) and $\mathbf{q}=\mathbf{c}^*/2$ (A point) of the original zone may become observable through light-scattering experiments in the sense that wave-vector conservation requirements are satisfied.

It has been observed experimentally that the inclusion of atoms or molecules between the planes of layered compounds does not significantly influence the vibrational frequencies of the atoms within the host layers.[6,15,24,25] Moreover, in a previous study on molecular single layers of MoS_2,[26] it was determined that the intralayer Raman modes were, to a first approximation, unaffected by the absence of the neighboring layers. This property of the vibrational modes in the transition-metal dichalcogenides can be explained by considering the differences between the weak van der Waals–type interlayer binding energy and the strong covalent-type intralayer bonds, which constitute the relevant force for the vibrational properties of the host. The effect of including foreign atoms within the interlayer gap upon the strength of the intralayer bonds is very small and, therefore, can be neglected to a good approximation. Moreover, it was also found[26] that the frequency of modes with certain symmetry did not vary significantly when the Mo atoms change coordination from trigonal prismatic to octahedral. In this case, the effect of changing the crystal symmetry affects the selection rules and optical activity of the vibrations with almost no variation of their vibrational frequencies.

Figure 1 shows the Raman spectra of stage-2 $Ag_{0.33}TiS_2$ single crystals obtained at 296, 240, and 15 K. An identical number of peaks were observed at the same positions in the spectra of ordered samples with $x=0.16$. The frequencies of the various lines are summarized in Table I. As the temperature is lowered, all the peaks become sharper and the broad feature appearing at ~ 205 cm^{-1} [Fig. 1(a)] is resolved into the D_3-D_4 doublet in the spectrum taken at 15 K [Fig. 1(c)]. It is interesting to note that the superlattice related peaks are already ob-

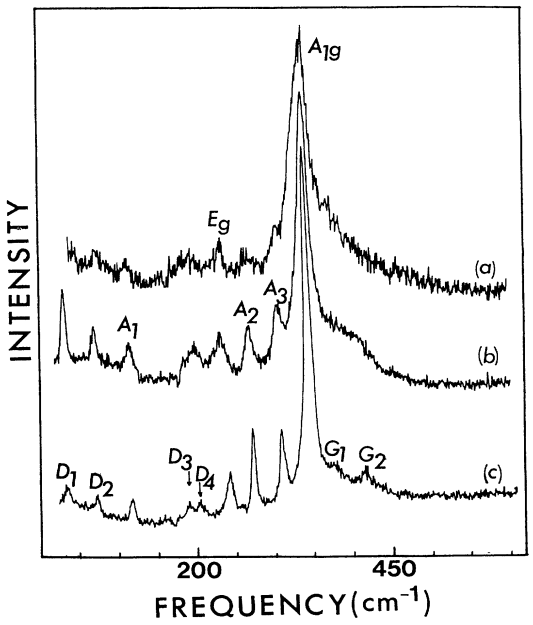

FIG. 1. Raman spectra of stage-2 $Ag_{0.33}TiS_2$ obtained at (a) 296 K, (b) 240 K, and (c) 15 K.

TABLE I. Frequencies (cm^{-1}), polarization, and assigned origin within the hexagonal TiS_2 Brillouin zone of the Raman-active modes observed in the spectra shown in Fig. 1.

Peak	Frequency (± 1 cm^{-1}) Temperature (K)			Polarization		Origin
	296	240	15	Experiment	Theory	
D_1	33	36	35	$(YY)+(YX)$	$(YY)+(YX)$	A
D_2	74	75	76	(YY)	(YY)	A
A_1	118	120	120	(YY)	(YY)	K
D_3			191	$(YY)+(YX)$	$(YY)+(YX)$	A
D_4	205	203	205	$(YY)+(YX)$	$(YY)+(YX)$	A
E_g	232	234	243	$(YY)+(YX)$	$(YY)+(YX)$	Γ
A_2	273	273	273	(YY)	$(YY)+(YX)$	K
A_3	308	308	310	(YY)	(YY)	A
A_{1g}	343	345	347	(YY)	(YY)	Γ
G_1			380		(YX)	K
G_2			415		$(YY)+(YX)$	K

servable, although not well defined, in the spectrum obtained at 296 K, which indicates that the onset of the phase transition must be slightly above 296 K, in agreement with the transition temperature previously reported ($T_c \cong 300$ K)[6,22] for $x \cong 0.33$. The temperature dependence of the peaks in the spectra from both $Ag_{0.33}TiS_2$ and $Ag_{0.16}TiS_2$ was similar to that observed[15,16] previously.

For comparison purposes, Raman spectra of unintercalated TiS_2 are shown in Fig. 2. At room temperature the frequency of the E_g and A_{1g} modes are 234 and 335 cm^{-1}, respectively, and at 15 K these frequencies shift to 244 and 339 cm^{-1}. In the TiS_2 spectra a broad shoulder appears on the high-energy side of the A_{1g} peak, which is also observable in the spectra of the intercalated samples (Fig. 1). The temperature dependence of this broad feature indicates that it originates from overtone and/or summation processes. As the temperature of the intercalated sample is lowered below ~ 150 K, two peaks, G_1 and G_2 in Fig. 1(c), rise above this second-order background. The intensities of G_1 and G_2 have a temperature dependence proportional to (n_j+1), where $n_j=[\exp(\hbar\omega_j/kT)-1]^{-1}$ is the Bose-Einstein occupation factor, which indicates that G_1 and G_2 are first-order phonons and, therefore, are also the result of the zone-folding mechanism.

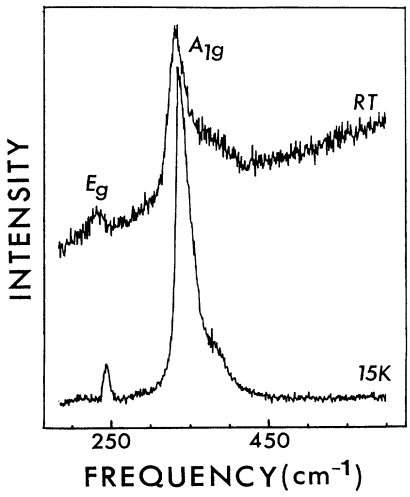

FIG. 2. Raman spectra of pure TiS_2 single crystals at room temperature and 15 K.

B. Lattice-dynamics calculations

A valence-force-field (VFF) lattice-dynamics model has been used to calculate the phonon-dispersion curves and phonon frequency distribution of TiS_2. In this material, the Ti atoms are octahedrally coordinated to the S atoms forming a structure whose symmetry is described by the space group D_{3d}^3 with the lattice constants $a=3.404$ Å and $c=5.690$ Å.[27] For our calculations, we have assumed an ideal geometry in which the c-axis component of the intralayer S-S distance is the same as the a spacing. The calculation has been performed by using a potential energy of the form $U=U_1+U_2$, where U_1 represents the intralayer potential energy given in terms of the force constants $K_r, K_m, K_\theta, K_\phi, K_\psi$ and $K_{rr'}^{\theta}$, by

$$U_1=\tfrac{1}{2}[K_r(\Delta r)^2+K_m(\Delta r_m)^2+K_\theta(r_0\Delta\theta)^2 + K_\phi(r_0\Delta\phi)^2+K_\psi(r_0\Delta\psi)^2+K_{rr'}^{\theta}(\Delta r\Delta r')^2] , \quad (1)$$

where r_0 is the equilibrium Ti—S bond length, r_m is the Ti-Ti distance, and $r, r', \theta, \phi, \psi$ are defined in a similar way as in Ref. 28 and are illustrated in Fig. 3 for the case of TiS_2. U_2 accounts for the interlayer interaction[29] and is given by

$$U_2=\tfrac{1}{2}[K_{R_1}(\Delta R_1)^2+K_{R_2}(\Delta R_2)^2] , \quad (2)$$

where R_1 and R_2 are the first and second nearest-neighbor distances between S atoms on opposite sides of the gap.

The calculation was performed by using the interatomic potential energy U within the Born-von Kármán approximation to calculate the eigenvectors and eigenfrequencies of the dynamical matrix. Table II lists the force constants obtained by fitting the calculated frequencies to

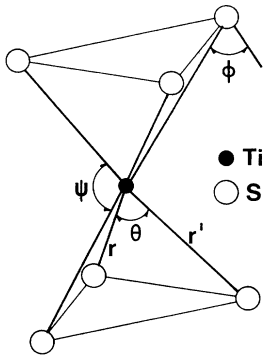

FIG. 3. Schematic diagram of octahedrally coordinated TiS_2. The bond angles and bond lengths employed in the lattice-dynamics calculation are indicated.

TABLE II. Force constants used in the lattice-dynamics calculation of TiS_2 in units of 10^4 dyn/cm.

Intralayer		Interlayer	
K_r	5.7577	K_{R_1}	0.1412
K_m	3.2545	K_{R_2}	0.1840
K_θ	1.2886		
K_ϕ	1.9741		
K_ψ	−1.5765		
$K^{\theta}_{rr'}$	−0.4935		

the available experimental data which include neutron scattering,[7] the room-temperature infrared[5] and Raman[6] frequencies of pure TiS_2, and the frequencies of the 296 K modes A_1, A_2, A_3, D_1, D_2, and D_4 along with those of G_1, G_2, and D_3 measured at 15 K (Table I). It can be noticed from Table I that, with the exception of the mode E_g, the frequencies of the observed Raman modes do not change significantly with temperature in the range investigated.

Figure 4 shows the calculated phonon-dispersion curves along the high-symmetry directions of the TiS_2 hexagonal Brillouin zone. The experimental data are also shown in Fig. 4 where the Raman frequencies have been indicated by solid squares. The fitting of the infrared and Raman frequencies at Γ was done by considering the symmetry of the dynamical matrix eigenvectors, while the assignment of the zone-folded modes to either the A or K points was done by considering the calculated frequencies at these points and by comparing the polarization properties of each peak, i.e., $\bar{Z}(YY)Z$ or $\bar{Z}(YX)Z$, with the expected polarizations derived from the Raman tensor polarization selection rules, which are determined by the space-group symmetry and the symmetry of the superstructure. Knowing[14] the occupied sites of the silver atoms above and below T_c, it can be found that the ordering of these atoms in the stage-2 phase is equivalent to a static distortion described by a totally symmetric "frozen-in" phonon. In accordance with the periodicity of the superlattice, this frozen-in phonon "propagates" with wave vectors $\mathbf{q}_1 \cong \mathbf{c}^*/2$ and $\mathbf{q}_2 = \frac{1}{3}(\mathbf{a}^* + \mathbf{b}^*)$ where $\mathbf{a}^*$, $\mathbf{b}^*$, and $\mathbf{c}^*$ refer to the unintercalated crystal. A zone-folded Raman mode can be described by a second-order process[30,31] involving the frozen-in phonon

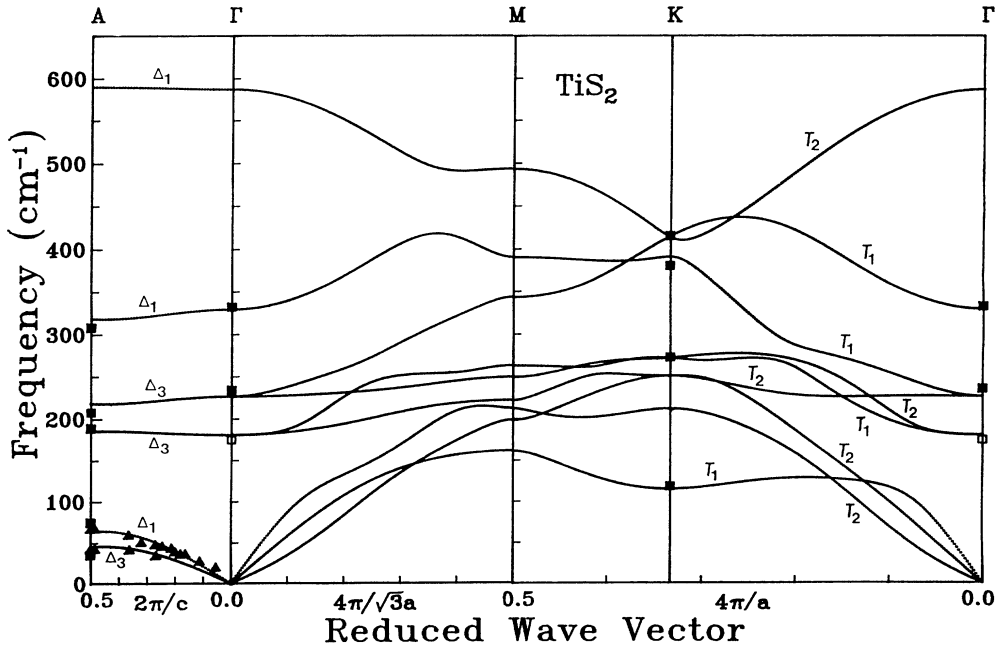

FIG. 4. Calculated phonon-dispersion curves of TiS_2 along the high-symmetry directions of the hexagonal Brillouin zone. The experimental data employed to adjust the force constants in the VFF model are shown for comparison purposes. Solid squares, Raman data; open squares, infrared E_u mode; solid triangles, neutron-scattering data. T_1, T_2 and Δ_1, Δ_3 label the irreducible representations of phonons along the Γ-K and Γ-A directions, respectively.

$\mathbf{Q}_0(\omega=0,-\mathbf{q}_0)$, responsible for the static distortion, and the dynamic phonon $\mathbf{Q}_\omega(\omega,\mathbf{q}_0)$, where ω is the Raman frequency and $\mathbf{q}_0=\mathbf{q}_1$ or $\mathbf{q}_2$. As a two-phonon process, the polarization selection rules can be worked out from the direct product of the irreducible representations of the two participating phonons,[32]

$$\Gamma_{Q_0,-q_0}\times\Gamma_{Q_\omega,q_0}\ . \tag{3}$$

The selection rules of all the zone-folded modes determined from (3) are given in the sixth column of Table I. It should be noted that according to the above analysis, the two modes at 211 cm^{-1} and 250 cm^{-1} at the K point (Fig. 4) should not be Raman active, in agreement with our observations. In fact, with the exception of the $A_{2u}(A)$ mode (Fig. 4) we have observed all the Raman modes at Γ, A, and K that are predicted by our calculations. From Table I it is observed that there is also good agreement between the predicted polarizations and the experiment. The only disagreement between our observation and the predictions obtained from (3) concerns the A_2 peak (Table I), which was not observed in the (YX) polarization geometry. This, however, could be due to small values of the corresponding Raman tensor elements, in which case the signal would be too weak to be detected.

Figure 5 shows the phonon density of states of TiS_2 obtained by counting the number of modes in a given frequency interval (1 cm^{-1}) of a fine grid formed by 228 900 points regularly distributed over $\frac{1}{24}$ of the Brillouin zone. This procedure yielded a reasonably accurate picture of the phonon frequency distribution, and interpolation methods[33] were not applied.

Negishi *et al.*,[9] using information gained from tunneling experiments, studied the phonon spectrum of TiS_2 for phonon energies lower than $\sim$200 cm^{-1}. The calculated phonon frequency distribution (Fig. 5) shows four peaks

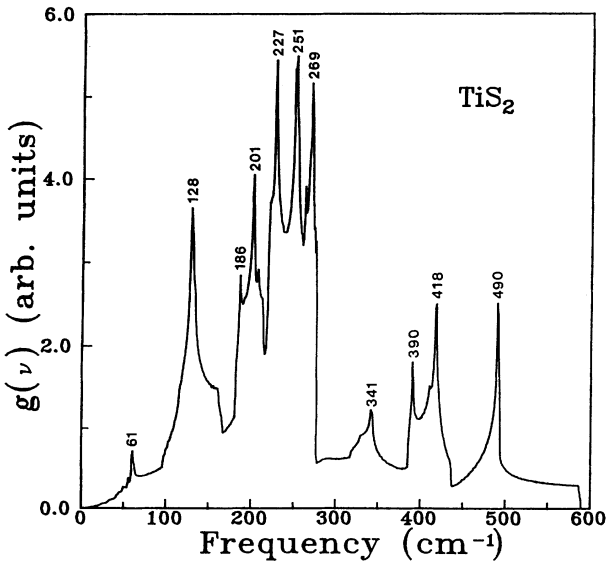

FIG. 5. Calculated phonon density of states of TiS_2 according to the VFF model.

for the same energy range at frequencies that agree well with the energy of the phonons at 8.2, 15.4, 24.4, and 24.7 meV reported by Negishi *et al.* On the other hand, the assignment of modes to the different Brillouin zone points in Negishi's paper differs from our results in that only about half of their reported values can be well accounted for at M and K in Fig. 4. This discrepancy is particularly noticeable for the low-energy modes, while the agreement with the higher-energy modes is more satisfactory. However, it is questionable whether or not this comparison is meaningful since Negishi *et al.*[9] assigned phonons to M, K, or A under the assumption that the dispersion curves of TiS_2 were similar to those of PbI_2, which is an ionic compound. In PbI_2 dipolar interactions play a major role in determining its vibrational properties,[34] in contrast to TiS_2 where screening of long-range Coulomb interactions by the free carriers must be taken into consideration as is discussed in the next section.

IV. DISCUSSION

We have employed a valence-force-field model to calculate the phonon dispersion curves of TiS_2. This model is appropriate for modeling the lattice dynamics of crystals in which the interatomic forces arise from contributions of a few near neighbors and where long-range Coulomb-type interactions are not important. On the other hand, from infrared spectroscopy studies[4,5] it has been deduced that the effective charge e_T^* in TiS_2 is rather large and equal to $6e$ ($5.9e$ in Ref. 5). Similar values of e_T^* have also been determined for other group-IV disulphides such as ZrS_2 and HfS_2 whose effective charges are $4.4e$ and $3.9e$, respectively. A consequence of such a large effective charge on the vibrational optical modes, in which the metal and chalcogenide atoms oscillate out of phase, is that they are no longer degenerate for longitudinal and transverse long-wavelength vibrations. This LO-TO splitting is manifested in the infrared spectra of ionic compounds in the form of Reststrahlen bands,[35] as observed in the infrared reflectance of ZrS_2 and HfS_2.[36] In accordance with the large e_T^* deduced for TiS_2 a large LO-TO splitting has been estimated for the E_u mode.[4,5] However, such a splitting has not been directly observed in the case of TiS_2. In this regard, there is experimental evidence in materials such as SnTe[37] and some transition-metal carbides[38,39] that a high density of free carriers an screen out the long-range Coulomb interactions that lead to the LO-TO splitting of the optic modes at $\mathbf{q}\cong 0$. In these materials deviations from stoichiometry produce a high density of free carriers which, for instance, in SnTe is of the order of 5×10^{20} holes/cm^3. In TiS_2 the density of free electrons is comparable[1] and for typical stoichoimetries ($Ti_{1.03}S_2$) is of the order of 5×10^{20} cm^{-3}. This large density of free electrons in TiS_2 effectively screens the long-range interaction originating from the ionic part of the Ti—S bonds and suppresses any LO-TO splitting for long-wavelength oscillations. Moreover, Cowley, Darby, and Pawley[37] used both a shell model modified to include screening effects, and a nonionic model to analyze their neutron-scattering

data of SnTe. They found that both of these models provided a good fit to the experimental data, a result that highlights the importance of screening in the lattice dynamics of compounds with carrier concentration similar to that of TiS_2. In the case of ZrS_2 and HfS_2 the densities of free carriers are of the order of 10^{18} and $<10^{17}$, respectively,[27] and screening effects are therefore not expected to play a dominant role.

Moreover, the ionic-versus-covalent nature in layered compounds has been analyzed by considering the relationship between structural parameters and ionic radii of the metal (M) and chalcogen (X) atoms. As indicated by Lucovsky *et al.*,[37] the M-X and X-X distances of the group-IV dichalcogenides ZrS_2, HfS_2, and $HfSe_2$ are consistent with an ionic description in the sense that those distances are very close to the sum of the ionic radii $r(M^{4+})+r(X^{2-})$ and $2r(X^{2-})$, respectively. However, the same approach is not as satisfactory when its applied to TiS_2 and group-VI covalent crystals MoS_2, $MoSe_2$, WS_2 and WSe_2.[36] It has been pointed out[36,40] that the ratio of the ionic radii r_+/r_- of sixfold-coordinated AB_2 compound falls between the boundaries 0.67 and 0.33 and that the above-mentioned MoS_2-type compounds have an r_+/r_- ratio in the 0.38–0.30 range, while for the more ionic, octahedrally coordinated compounds this ratio is larger. For example, the group-IV dichalcogenides ZrS_2 and HfS_2 have a $r(M^{4+})/r(X^{2-})$ ratio equal to 0.43 and 0.42, respectively, whereas for TiS_2 this ratio equals 0.37, a value that lies within the range of the more covalent-type compounds.

From the above-mentioned considerations, we have assumed that screening of the ionic fraction of the Ti—S bonds by the large free-carrier density of TiS_2 plays a major role in the vibrational properties of this material and that its lattice dynamics can be described satisfactorily by a VFF model, which has been successfully used in the past to calculate the phonon-dispersion curves of other transition-metal dichalcogenides such as MoS_2,[26,28] $TaSe_2$,[41] $NbSe_2$,[41,42] and WS_2.[43]

Finally, to the best of the authors' knowledge, there is no experimental report on the frequency of the infrared active A_{2u} mode, in which the Ti and S atoms oscillate along the direction perpendicular to the layer. It has not been possible to measure this mode directly because the crystals grown so far are not thick enough to enable reliable c-axis reflectivity measurements. For the purposes of comparison, however, an estimate of this frequency can be obtained from mass scaling the A_{2u} mode of 2H-MoS_2, since the period of oscillation of a vibration with certain symmetry does not vary significantly when the coordination is changed from trigonal prismatic to octahedral.[26] By doing so, one obtains a frequency of 560 cm^{-1} for the A_{2u} mode of TiS_2 which compares well with 587 cm^{-1} obtained in our calculation, Fig. 4.

V. CONCLUSIONS

Raman-scattering experiments have been performed in stage-2 $Ag_{0.33}TiS_2$ and $Ag_{0.16}TiS_2$ crystals which undergo an order-disorder phase transition that results in the formation of a $\sqrt{3}a\times\sqrt{3}a\times 2c$ superlattice. Due to improved experimental conditions and sample surface quality, five new Raman modes were observed in addition to the E_g and A_{1g} modes of pure TiS_2 and the A_1, A_2, A_3, and D_4 modes reported in previous experiments[6,15,16] on electrochemically silver-intercalated TiS_2 samples. The additional features in the spectra can be explained in terms of the zone-folding mechanism that occurs after the superlattice is formed. According to the superperiodicity, the new Raman peaks correspond to phonons at the K and A points of the TiS_2 Brillouin zone. The 11 observed Raman frequencies, in addition to infrared[5] and neutron-scattering data,[7] were utilized to determine the parameters of a valence-force-field lattice-dynamics model, which was used to calculate the phonon-dispersion curves and phonon density of states of TiS_2. The application of this model has assumed that the ionic part of the Ti—S bonds is effectively screened by the large density of free carriers in TiS_2. This assumption appears warranted by the results obtained in other materials with comparable free carrier density and bond ionicity, and by the good agreement obtained between the model predictions and the available experimental data in TiS_2. It is believed that the model developed in this work should also be useful in describing the lattice dynamics of other octahedrally coordinated layer structures with carrier concentrations in excess of 10^{20} cm^{-3} such as $HfTe_2$, $ZrTe_2$, $NbTe_2$, and $TaTe_2$.

ACKNOWLEDGMENTS

We would like to thank Dr. K. K. Bardhan for growing the intercalated crystals and Dr. R. F. Frindt and Mr. P. Joensen for preparing the pure TiS_2 samples. The authors have also benefited from helpful discussions with Dr. R. R. Frindt. The financial support of the Natural Sciences and Engineering Research Council of Canada is gratefully acknowledged.

*On leave of absence from Departamento de Física, Centro de Investigación y de Estudios Avanzados del Instituto Politécnico Nacional, Apartado Postal 14-740, México 07000, Distrito Federal, Mexico.

[1]P. C. Klipstein, A. G. Bagnall, W. Y. Liang, E. A. Marseglia, and R. H. Friend, J. Phys. C **14**, 4067 (1981).

[2]J. Molenda, A. Stoklosa, S. Mrowec, and Do Than, Phys. Status Solidi A **119**, 571 (1990).

[3]J. A. Wilson, Phys. Status Solidi B **86**, 11 (1978).

[4]H. P. Vaterlaus and F. Lévy, J. Phys. C **18**, 2351 (1985).

[5]G. Lucovsky, W. Y. Liang, R. M. White, and K. R. Pisharody, Solid State Commun. **19**, 303 (1976).

[6]W. K. Unger, J. M. Reyes, O. Singh, A. E. Curzon, J. C. Irwin, and R. F. Frindt, Solid State Commun. **28**, 109 (1978).

[7]M. Schärli and F. Lévy, Phys. Rev. B **33**, 4317 (1986).
[8]M. Kaveh, M. F. Cherry, and M. Weger, J. Phys. C **14**, L789 (1981).
[9]H. Negishi, M. Marushita, M. Koyano, and M. Inoue, J. Low Temp. Phys. **73**, 459 (1988).
[10]J. Dijstra, C. F. van Bruggen, and C. Haas, J. Phys. Condens. Matter **1**, 4297 (1989).
[11]M. Inoue, H. P. Hughes, and A. D. Yoffe, Adv. Phys. **38**, 565 (1989).
[12]K. Kawano, J. Takahashi, R. Nakata, and M. Sumita, J. Phys. Soc. Jpn. **58**, 949 (1989).
[13]G. A. Wiegers, K. D. Bronsema, S. Van Smaalen, R. J. Haange, J. E. Zondag, and J. L. de Boer, J. Solid State Chem. **67**, 9 (1987).
[14]G. A. Scholz and R. F. Frindt, Mater. Res. Bull. **15**, 1703 (1980).
[15]M. Plischke, K. K. Bardhan, R. Leonelli, and J. C. Irwin, Can. J. Phys. **61**, 397 (1983).
[16]R. Leonelli, M. Plischke, and J. C. Irwin, Phys. Rev. Lett. **45**, 1291 (1980).
[17]B. G. Silbernagel and M. S. Whittingham, Mater. Res. Bull. **11**, 29 (1976).
[18]A. H. Thompson, Phys. Rev. Lett. **40**, 1511 (1978).
[19]J. I. Meakin, P. C. Klipstein, and R. H. Friend, J. Phys. C **20**, 271 (1987).
[20]K. K. Bardhan, G. Kriczenow, and J. C. Irwin, J. Phys. C **18**, L131 (1985).
[21]See also, for example, D. Kaluarachi and R. F. Frindt, Phys. Rev. B **28**, 3663 (1983) and S. A. Safran, Solid State Phys. **40**, 183 (1987), and references therein.
[22]A. G. Gerards, H. Roede, R. J. Haange, B. A. Boukamp, G. A. Wiegers, Synth. Met. **10**, 51 (1984).
[23]R. M. Suter, M. W. Shafer, P. M. Horn, and P. Dimon, Phys. Rev. B **26**, 1495 (1982).
[24]J. C. Tsang and M. W. Shafer, Solid State Commun. **25**, 999 (1978).
[25]M. S. Dresselhaus, D. Dresselhaus, P. C. Eklund, and D. D. L. Chung, Mater. Sci. Eng. **31**, 141 (1977).
[26]S. Jiménez-Sandoval, D. Yang, R. F. Frindt, and J. C. Irwin, Phys. Rev. B **44**, 3955 (1991).
[27]A. Wilson and A. D. Yoffe, Adv. Phys. **18**, 193 (1969).
[28]N. Wakabayashi, H. G. Smith, and R. M. Nicklow, Phys. Rev. B **12**, 659 (1975).
[29]J. L. Feldman and L. L. Boyer, Solid State Commun. **37**, 879 (1981).
[30]X. K. Chen, W. K. Lee, J. S. Hwang, and H. Z. Cummins, Phys. Rev. B **42**, 8465 (1990).
[31]H. Poulet and R. M. Pick, J. Phys. C **14**, 2675 (1981).
[32]W. Hayes and R. Loudon, *Scattering of Light by Crystals* (Wiley, New York, 1978).
[33]L. J. Raubenheimer and G. Gilat, Phys. Rev. **157**, 586 (1967).
[34]A. Frey and R. Zeyher, Solid State Commun. **28**, 435 (1978).
[35]P. M. A. Sherwood, *Vibrational Spectroscopy of Solids* (Cambridge University Press, Cambridge, England, 1972), p. 83.
[36]G. Lucovsky, R. M. White, J. A. Benda, and J. F. Revelli, Phys. Rev. B **7**, 3859 (1973).
[37]E. R. Cowley, J. K. Darby, and G. S. Pawley, J. Phys. C. **2**, 1916 (1969).
[38]H. G. Smith and W. Gläser, Phys. Rev. Lett. **25**, 1611 (1970).
[39]W. Weber, Phys. Rev. B **8**, 5082 (1973).
[40]C. Y. Fong and M. Schlüter, in *Electrons and Phonons in Layered Crystal Systems,* edited by T. J. Wieting and M. Schlüter (Reidel, Dordrecht, Holland, 1979).
[41]J. L. Feldman, Phys. Rev. B **25**, 7132 (1982).
[42]N. Wakabayashi and R. M. Nicklow, in *Electrons and Phonons in Layered Crystal Systems* (Ref. 40).
[43]C. Sorisseau, F. Cruege, and M. Fouassier, Chem. Phys. **150**, 281 (1991).